Hindawi
Structural Control and Health Monitoring
Volume 2023, Article ID 5569434, 15 pages
https://doi.org/10.1155/2023/5569434

Research Article

Accurate Modeling and Wave Propagation Analysis of Cracked Slender Structural Members by the Spectral Element Method

Fushou Liu, Aobo Liu, Libin Wang, and Yang Wei

College of Civil Engineering, Nanjing Forestry University, 210037 Nanjing, China

Correspondence should be addressed to Yang Wei; wy78@njfu.edu.cn

Received 27 November 2022; Revised 30 March 2023; Accepted 17 April 2023; Published 5 May 2023

Academic Editor: Chia-Ming Chang

The analysis of elastic wave propagation in cracked structures is very useful in the crack detection by the ultrasonic guided wave method. This study presents an accurate spectral element modeling method for cracked slender structural members by using refined waveguide models and a more realistic crack model. Firstly, a spatial spectral beam element model is established for uncracked slender structural member based on the Love rod theory, the modified Timoshenko beam theory, and the Saint-Venant's torsion theory. Then, the complete local additional flexibility matrix for crack in the structural member with rectangular cross section is derived from the theory of elastic fracture mechanics, and a two-node condensed spectral element model considering the stiffness coupling effect caused by the crack is established for cracked slender structural member. The wave response in cracked structures is solved by the numerical inverse Laplace transformation method. A thorough comparison of the wave responses in cracked structural member evaluated by the presented spectral element model and the 3D solid finite element model is given in the numerical example, which verifies the accuracy and high efficiency of the presented method.

1. Introduction

Transverse cracks often occur in structural members during the service of structures, which poses a threat to the safety of the structures. Efficient and accurate detection of cracks in structures is an important task in the field of structural health monitoring [1, 2]. The appearance of cracks leads to changes in the local stiffness of the structure, thus changing the overall dynamic characteristics of the structure. Therefore, many researchers have proposed various methods to detect structural crack damage based on modal parameters and vibration responses [3–5]. However, these methods also have some shortcomings; for example, modal parameters are insensitive to local minor damage of structure, and structural vibration response is easily disturbed by low frequency environmental vibration, etc. [6, 7]. In recent years, the nondestructive detection method of structures based on ultrasonic guided waves has attracted much attention due to its remarkable advantages [8–13].

In the past few decades, many researchers have studied the modeling and analysis of cracked structures. When cracks occur in a structural member, additional local flexibility will be generated in the member. Papadopoulos and Dimarogonas [14] proposed a method for calculating the local flexibility matrix of cracked beams based on the laws of fracture mechanics and pointed out that the local flexibility matrix contains nonzero nondiagonal elements which yields the coupling of axial vibration and bending vibration of the beams. Zheng and Kessissoglou [15] used an "overall additional flexibility matrix" instead of the "local additional flexibility matrix" in the derivation of the stiffness matrix of a cracked beam element by the finite element method (FEM) and analyzed the free vibration of cracked beams. Muscolino and Santoro [16] used FEM to analyze the dynamic response of beams with multiple cracks under deterministic and random loads. Mousavi et al. [17] proposed a damage identification method for beam structures by quaternion analysis of beam multitype vibration data and modeling the crack as a zero-length spring located between two standard beam elements, with rotational and translational stiffnesses. The above-given studies are all aimed at the low frequency vibration of the cracked structures. For simulation of high

frequency wave propagation in structures, such as the ultrasonic guided wave, the traditional FEM has encountered some problems such as numerical dispersion error and prohibitive computational cost [18].

The spectral element method (SEM) combines the complex geometric adaptability of the FEM and the rapid convergence characteristic of the spectral method, is an effective method for wave propagation analysis of structures [19–22]. The conventional SEM based on the fast Fourier transform (FFT) can obtain accurate result in the frequency domain, but it is easy to have aliasing or leakage errors in the time domain solution because the use of inverse FFT. To avoid these errors, the conventional SEM uses artificial damping or throw-off element [19, 20]. Several other approaches have also been proposed, such as the SEM based on the Laplace transform [21], the Wavelet based spectral finite element method [22], and the imaginary spectral element method [23].

In the areas of wave propagation analysis in cracked slender structures, Palacz and Krawczuk [24] modeled the crack as a massless axial spring and used the SEM to study the propagation of longitudinal waves in cracked rod. Lucena and Dos Santos [25] used the SEM and time reversal method to detect and locate the damage of cracked rod by modeling the crack as an axial spring. Krawczuk et al. [26] studied the propagation of flexural wave in a cracked Timoshenko beam with rectangular cross section by modeling the crack as a dimensionless and massless spring with bending and shear flexibilities. Xu et al. [27] established the SEM model of Euler–Bernoulli beam with multiple cracks by modeling the crack as a massless spring with bending flexibility. Izadifard et al. [28] modelled the crack as massless rotational and translational springs and established the dynamic model of cracked frame structure by the SEM. Ritdumrongkul and Fujino [29] established a cracked Timoshenko beam spectral element model in which the crack was modelled by shifting the neutral axis of the beam. Although the SEM has been used in wave propagation analysis of cracked structures in the above-given studies, there are still two critical issues need to be further studied. The first one is that the structural members were all modeled by simplified waveguide models (such as the elementary rod model and the classical Euler–Bernoulli beam or Timoshenko beam model) and the stiffness coupling effect caused by the crack was neglected in the previous studies, which inevitably lead to errors in the simulation results, especially for simulation of high frequency wave such as the ultrasonic guided wave. The second one is that a thorough comparison between the wave responses obtained by the spectral element models and those obtained by experiments or 3D solid FEM models was lacked in the previous studies.

In this study, an accurate spectral element modeling method was presented for cracked structural members based on refined waveguide theory and considering the stiffness coupling effect caused by the crack; furthermore, a thorough comparison between the wave response obtained by the spectral element model and the 3D solid finite element model was made. In Section 2, the spectral element model was established based on the Love rod theory, the modified Timoshenko beam theory, and the Saint-Venant's torsion theory, firstly. Then, the local flexibility matrix caused by the crack was derived from the strain energy release rete. A two-node condensed spectral element model for the cracked structural member was established and the wave response of the cracked structure was solved by numerical inverse Laplace transformation method. In Section 3, numerical example was given to verify the correctness of the presented modeling method and analyze the propagation behavior of ultrasonic guided wave in cracked structural members. In Section 4, conclusions are given.

2. Theoretical Modeling

As shown in Figure 1, a straight structural member with an open crack is considered in this study. The length of the member is l, and the distances between the crack and the two ends of the member are l_a and l_b, respectively. The dynamic model of this cracked member is established by the spectral element method, in which the left and right sides of the crack are modelled as a spatial beam element, respectively, and the crack is modeled as a massless elastic connection element.

2.1. Spectral Element Model of the Uncracked Structural Member. The classical continuum mechanics models such as the elementary rod model and the Euler–Bernoulli beam model are proved to be suitable for analyzing most of static and vibration problems of slender structures [13, 30]. However, these elementary models may encounter problems in some special engineering fields, such as micro- and nanostructures [31, 32], lattice structures [33], and high-frequency wave propagation analysis [34]. To overcome these problems, some refined models or higher-order models are usually resorted.

For analyzing the propagation of longitudinal wave in a slender structural member, the elementary rod model was often used in previous studies, which gives the following wave equation:

$$EA\frac{\partial^2 u}{\partial x^2} - \rho A\frac{\partial^2 u}{\partial t^2} = 0, \tag{1}$$

where E and ρ are the Young's modulus and density of the material, A is the area of the cross section. However, the elementary rod theory ignores the lateral expansion and contraction of the cross section of structural member caused by the Poisson's ratio effect, which will bring error in simulating the propagation of longitudinal wave in structural member. Alternatively, the Love rod theory considers the above-given Poisson's ratio effect by calculating additional kinetic energy due to lateral motion, and the wave equation takes the following form [19, 34]:

$$EA\frac{\partial^2 u}{\partial x^2} + \nu^2\rho J\frac{\partial^4 u}{\partial x^2\partial t^2} - \rho A\frac{\partial^2 u}{\partial t^2} = 0, \tag{2}$$

where ν is Poisson's ratio, J is the polar moment of inertia of the cross section of the member.

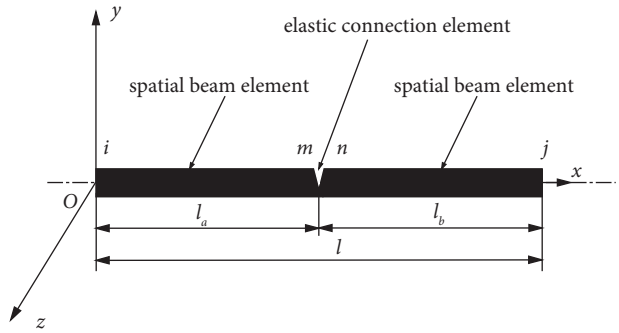

Figure 1: Spectral element model of the cracked structural member.

According to equation (2) and using the spectral element method based on Laplace transformation [21], the equation of longitudinal wave motion of the structural member can be written as

$$\mathbf{S}_l(s)\mathbf{u}_l(s) = \mathbf{F}_l(s), \tag{3}$$

where $\mathbf{u}_l(s) = \left\{\widehat{u}_i, \widehat{u}_j\right\}^{\mathrm{T}}$ and $\mathbf{F}_l(s) = \left\{\widehat{F}_{xi}, \widehat{F}_{xj}\right\}^{\mathrm{T}}$ are the nodal displacement vector and nodal load vector for longitudinal motion of the member after Laplace transformation, respectively, the variables with overhead symbol "^" denotes the Laplace transform of the corresponding variables in the time domain, the subscripts i an j are the number of the nodes of the spectral element

$$\mathbf{S}_l(s) = \frac{EA}{l}\begin{bmatrix} k_x l\cot(k_x l) & -k_x l\csc(k_x l) \\ -k_x l\csc(k_x l) & k_x l\cot(k_x l) \end{bmatrix}, \tag{4}$$

where

$$k_x = \mathrm{i}s\sqrt{\frac{\rho A}{EA + s^2\nu^2\rho J}}, \tag{5}$$

the complex variable $s = \sigma + \mathrm{i}\omega$ is the Laplace transform parameter, σ is a positive real constant, ω is the circular frequency, $\mathrm{i} = \sqrt{-1}$ is the imaginary unit.

For analysis of the propagation of high frequency flexural wave in the structural member, the Timoshenko beam model is usually adopted. However, the classical Timoshenko beam model also has some differences with the behavior of wave propagation in real structure, the modified Timoshenko beam model is used here. Taking the transverse motion around the y-axis as an example,

$$K_1 GA\left(\frac{\partial^2 w}{\partial x^2} - \frac{\partial \theta_y}{\partial x}\right) - \rho A\frac{\partial^2 w}{\partial t^2} = 0, \tag{6}$$

$$EI_y\frac{\partial^2 \theta_y}{\partial x^2} + K_1 GA\left(\frac{\partial w}{\partial x} - \theta_y\right) - K_2\rho I_y\frac{\partial^2 \theta_y}{\partial t^2} = 0, \tag{7}$$

where I_y is the area moment of inertia of the cross section around the y-axis, G is the shear modulus, w, and θ_y are the transverse displacement and rotation of the cross section, respectively; K_1 and K_2 are the correction coefficients. The choose of the correction coefficients has different criterions, a suggested selection method for the correction coefficients is [19]

$$K_1 = \left(\frac{0.87 + 1.12\nu}{1 + \nu}\right)^2, \qquad K_2 = \frac{12K_1}{\pi^2}, \tag{8}$$

which matches the cut-off frequency of the modified Timoshenko beam model with that of the Lamb mode. The correction coefficients can be adjusted to give the best correspondence with the experimental results in the considered frequency range [6], so the following expressions are used here instead of equation (8):

$$K_1 = \eta_1\left(\frac{0.87 + 1.12\nu}{1 + \nu}\right)^2, \qquad K_2 = \frac{12K_1}{\pi^2}, \tag{9}$$

where η_1 is an adjustment coefficient.

According to equations (6) and (7) and using the spectral element method based on Laplace transformation, the equation of transverse wave motion of the structural member can be written as

$$\mathbf{S}_{by}(s)\mathbf{u}_{by}(s) = \mathbf{F}_{by}(s), \tag{10}$$

where $\mathbf{u}_{by}(s) = \left\{\widehat{w}_i, \widehat{\theta}_{yi}, \widehat{w}_j, \widehat{\theta}_{yj}\right\}^{\mathrm{T}}$ and $\mathbf{F}_{by}(s) = \left\{\widehat{F}_{zi}, \widehat{M}_{yi}, \widehat{F}_{zj}, \widehat{M}_{yj}\right\}^{\mathrm{T}}$ are the nodal displacement vector and nodal load vector for transverse motion of the member after Laplace transformation, respectively,

$$\mathbf{S}_{by} = EI_y\begin{bmatrix} F_{1y} & F_{2y} & F_{3y} & -F_{4y} \\ & F_{5y} & F_{4y} & F_{6y} \\ & & F_{1y} & -F_{2y} \\ \mathrm{sym} & & & F_{5y} \end{bmatrix}, \tag{11}$$

where

$$
\begin{aligned}
F_{1y} &= -\mathrm{i}\frac{r_{ty}r_{ey}}{\Delta_y}\left[\left(e_{ty}^2-1\right)\left(e_{ey}^2+1\right)r_{ty}-\left(e_{ty}^2+1\right)\left(e_{ey}^2-1\right)r_{ey}\right]\left(k_{ty}r_{ty}-k_{ey}r_{ey}\right)\\
F_{2y} &= \frac{-r_{ty}r_{ey}}{\Delta_y}\left\{\left(e_{ty}^2-1\right)\left(e_{ey}^2-1\right)\left(k_{ty}r_{ey}+k_{ey}r_{ty}\right)-\left[\left(e_{ty}^2+1\right)\left(e_{ey}^2+1\right)-4e_{ty}e_{ey}\right]\left(k_{ty}r_{ty}+k_{ey}r_{ey}\right)\right\}\\
F_{3y} &= 2\mathrm{i}\frac{r_{ty}r_{ey}}{\Delta_y}\left[\left(e_{ty}^2-1\right)e_{ey}r_{ty}-\left(e_{ey}^2-1\right)e_{ty}r_{ey}\right]\left(-k_{ty}r_{ty}+k_{ey}r_{ey}\right)\\
F_{4y} &= -2\frac{r_{ty}r_{ey}}{\Delta_y}\left(e_{ty}-e_{ey}\right)\left(1-e_{ty}e_{ey}\right)\left(-k_{ty}r_{ty}+k_{ey}r_{ey}\right)\\
F_{5y} &= -\mathrm{i}\frac{\left(k_{ty}r_{ty}-k_{ey}r_{ey}\right)}{\Delta_y}\left[-\left(e_{ty}^2+1\right)\left(e_{ey}^2-1\right)r_{ty}+\left(e_{ty}^2-1\right)\left(e_{ey}^2+1\right)r_{ey}\right]\\
F_{6y} &= -2\mathrm{i}\frac{\left(k_{ty}r_{ty}-k_{ey}r_{ey}\right)}{\Delta_y}\left[\left(e_{ey}^2-1\right)e_{ty}r_{ty}-\left(e_{ty}^2-1\right)e_{ey}r_{ey}\right]\\
\Delta_y &= 2r_{ty}r_{ey}\left[\left(e_{ty}^2+1\right)\left(e_{ey}^2+1\right)-4e_{ty}e_{ey}\right]-\left(r_{ty}^2+r_{ey}^2\right)\left(e_{ty}^2-1\right)\left(e_{ey}^2-1\right)\\
e_{ty} &= e^{-\mathrm{i}k_{ty}L},\ e_{ey}=e^{-\mathrm{i}k_{ey}L}\\
r_{ty} &= k_{ty}{}^{-1}\left(k_{ty}^2+s^2\rho A/K_1\mathrm{GA}\right),\ r_{ey}=k_{ey}{}^{-1}\left(k_{ey}^2+s^2\rho A/\mathrm{K_1GA}\right)\\
k_{ty} &= \frac{1}{\sqrt{2}}\sqrt{-\left(\frac{K_2\rho I_y}{EI_y}+\frac{\rho A}{K_1GA}\right)s^2+\sqrt{\left(\frac{K_2\rho I_y}{EI_y}-\frac{\rho A}{K_1GA}\right)^2s^4-4\frac{\rho I_y}{EI_y}s^2}}\\
k_{ey} &= \frac{1}{\sqrt{2}}\sqrt{-\left(\frac{K_2\rho I_y}{EI_y}+\frac{\rho A}{K_1GA}\right)s^2-\sqrt{\left(\frac{K_2\rho I_y}{EI_y}-\frac{\rho A}{K_1GA}\right)^2s^4-4\frac{\rho I_y}{EI_y}s^2}}
\end{aligned}
\tag{12}
$$

For analyzing the propagation of torsional wave in the structural member, the Saint-Venant's torsion theory [35] is adopted to consider the warping of the member with noncircular cross section, and the wave equation is

$$
S_t\frac{\partial^2\theta_x}{\partial x^2}-\rho J\frac{\partial^2\theta_x}{\partial t^2}=0, \tag{13}
$$

where S_t is the torsional stiffness of the member, which can be evaluated as follows [35]:

$$
S_t=\iint_A G\left[\left(\frac{\partial\psi}{\partial y}-z\right)^2+\left(\frac{\partial\psi}{\partial z}+y\right)^2\right]\mathrm{d}A, \tag{14}
$$

where ψ is the warping function.

Based on equation (13), the equation of torsional motion of the structural member can be obtained as

$$
\mathbf{S}_t(s)\mathbf{u}_t(s)=\mathbf{F}_t(s), \tag{15}
$$

where $\mathbf{u}_t(s)=\left\{\widehat{\theta}_{xi},\widehat{\theta}_{xj}\right\}^T$ and $\mathbf{F}_t(s)=\left\{\widehat{M}_{xi},\widehat{M}_{xj}\right\}^T$ are the nodal displacement vector and nodal load vector for torsional wave motion of the member after Laplace transformation, respectively,

$$
\begin{aligned}
\mathbf{S}_t(s) &= \frac{S_t}{l}\begin{bmatrix} k_tl\cot\left(k_tl\right) & -k_tl\csc\left(k_tl\right)\\ -k_tl\csc\left(k_tl\right) & k_tl\cot\left(k_tl\right)\end{bmatrix},\\
k_t &= \mathrm{i}s\sqrt{\frac{\rho J}{S_t}}.
\end{aligned}
\tag{16}
$$

Combining the spectral element equations describing the longitudinal wave motion, the transverse wave motion and the torsional wave motion of the structural member, the equations of motion of the spatial spectral beam element model of the structural member can be written as

$$
\mathbf{S}_B(s)\mathbf{u}_B(s)=\mathbf{F}_B(s), \tag{17}
$$

where

$$\begin{aligned}\mathbf{u}_B(s) &= \left\{\widehat{u}_i, \widehat{v}_i, \widehat{w}_i, \widehat{\theta}_{xi}, \widehat{\theta}_{yi}, \widehat{\theta}_{zi}, \widehat{u}_j, \widehat{v}_j, \widehat{w}_j, \widehat{\theta}_{xj}, \widehat{\theta}_{yj}, \widehat{\theta}_{zj}\right\}^{\mathrm{T}},\\ \mathbf{F}_B(s) &= \left\{\widehat{F}_{xi}, \widehat{F}_{yi}, \widehat{F}_{zi}, \widehat{M}_{xi}, \widehat{M}_{yi}, \widehat{M}_{zi}, \widehat{F}_{xj}, \widehat{F}_{yj}, \widehat{F}_{zj}, \widehat{M}_{xj}, \widehat{M}_{yj}, \widehat{M}_{zj}\right\}^{\mathrm{T}}.\end{aligned} \tag{18}$$

In order to consider the effect of damping in the simulation of the high-frequency wave propagation in the structural members, the complex modulus method is often used [36–38]. The exact complex modulus of material is a function of the vibration frequency [39, 40].

$$E^*(\omega) = E(\omega)[1 + \eta(\omega)], \tag{19}$$

where $E(\omega)$ and $\eta(\omega)$ are frequency-dependent Young's modulus and loss factor, respectively. There are different models for expressing $E(\omega)$ and $\eta(\omega)$ with frequency ω; however, the coefficients in the formulas of these models for different materials need to be determined throughout experimental testing. In simulation study, an approximation method was often used which adopts constant Young's modulus and loss factor instead of the frequency-dependent ones [37, 38].

2.2. Spectral Element Model of the Crack. The calculation of the additional flexibility caused by the crack in structural member is related to the section type of the member. Taking the member with rectangular cross section shown in Figure 2 as an example, the height and width of the cross section are b and h, respectively, the depth of the crack is a. By using the theory of fracture mechanics and calculating the additional strain energy produced by the crack, the additional flexibility coefficient at the crack position can be obtained.

According to the theory of elastic fracture mechanics, the strain energy release rate for the crack is as follows [3, 14]:

$$J_E = \frac{1}{E'}\left[\left(\sum_{i=1}^{6} K_{\mathrm{I}i}\right)^2 + \left(\sum_{i=1}^{6} K_{\mathrm{II}i}\right)^2 + m\left(\sum_{i=1}^{6} K_{\mathrm{III}i}\right)^2\right], \tag{20}$$

where $E' = E/(1-\nu^2)$, $m = 1/(1-\nu)$, the subscript I, II, and III represent three basic modes of fracture, namely, the opening mode, the sliding mode, and the tearing mode [41]; the stress intensity factors corresponding to the three modes are as follows [3]:

$$\begin{aligned}
&K_{\mathrm{I}1} = \frac{P_1}{hb}\sqrt{\pi\xi}F_1(\bar{\xi}), K_{\mathrm{I}5} = \frac{12P_5 z}{hb^3}\sqrt{\pi\xi}F_1(\bar{\xi}),\\
&K_{\mathrm{I}6} = \frac{6P_6}{h^2 b}\sqrt{\pi\xi}F_2(\bar{\xi}), K_{\mathrm{I}2} = K_{\mathrm{I}3} = K_{\mathrm{I}4} = 0,\\
&K_{\mathrm{II}2} = \frac{\beta_z P_2}{hb}\sqrt{\pi\xi}F_{\mathrm{II}}(\bar{\xi}), K_{\mathrm{II}4} = \frac{\phi_y P_4}{hb}\sqrt{\pi\xi}F_{\mathrm{II}}(\bar{\xi}),\\
&K_{\mathrm{II}1} = K_{\mathrm{II}3} = K_{\mathrm{II}5} = K_{\mathrm{II}6} = 0,\\
&K_{\mathrm{III}3} = \frac{\beta_y P_3}{hb}\sqrt{\pi\xi}F_{\mathrm{III}}(\bar{\xi}), K_{\mathrm{III}4} = \frac{\phi_z P_4}{hb}\sqrt{\pi\xi}F_{\mathrm{III}}(\bar{\xi})\\
&K_{\mathrm{III}1} = K_{\mathrm{III}2} = K_{\mathrm{III}5} = K_{\mathrm{III}6} = 0,
\end{aligned} \tag{21}$$

with the correction functions [14, 15],

$$F_1(\bar{\xi}) = \frac{\sqrt{(2/\pi\bar{\xi})\tan(\pi\bar{\xi}/2)}\left[0.752 + 2.02\bar{\xi} + 0.37(1-\sin(\pi\bar{\xi}/2))^3\right]}{\cos(\pi\bar{\xi}/2)}, \tag{22}$$

$$F_2(\bar{\xi}) = \frac{\sqrt{(2/\pi\bar{\xi})\tan(\pi\bar{\xi}/2)}\left[0.923 + 0.199(1-\sin(\pi\bar{\xi}/2))^4\right]}{\cos(\pi\bar{\xi}/2)}, \tag{23}$$

$$F_{\mathrm{II}}(\bar{\xi}) = \frac{1.122 - 0.561\bar{\xi} + 0.085\bar{\xi}^2 + 0.180\bar{\xi}^3}{\sqrt{1-\bar{\xi}}}, \tag{24}$$

$$F_{\mathrm{III}}(\bar{\xi}) = \sqrt{\frac{2}{\pi\bar{\xi}}\tan\left(\frac{\pi\bar{\xi}}{2}\right)}, \tag{25}$$

where P_1,..., P_6 are the internal forces of the structural member, whose definitions are shown in Figure 2(a), β_y and β_z are shear shape coefficients of the cross section, ϕ_y and ϕ_z are functions describing the stress distribution during torsion of the cross section, $\bar{\xi} = \xi/h$.

The additional flexibility coefficients caused by the crack can be evaluated from the strain energy release rate as

$$C_{ij} = \frac{\partial^2}{\partial P_i \partial P_j}\int_{-b/2}^{b/2}\int_0^a J_E(\xi)\mathrm{d}\xi\,\mathrm{d}\eta,\ (i, j = 1, 2, \ldots 6). \tag{26}$$

Substituting equation (20) into (26) yields

$$\begin{aligned} C_{11} &= \frac{2\pi}{E'b}\int_0^{\bar{a}} F_1(\bar{\xi})^2\bar{\xi}\mathrm{d}\bar{\xi}\int_{-1/2}^{1/2}\mathrm{d}\bar{\eta} \\ C_{22} &= \frac{2\pi\beta_z{}^2}{E'b}\int_0^{\bar{a}} F_{\mathrm{II}}(\bar{\xi})^2\bar{\xi}\mathrm{d}\bar{\xi}\int_{-1/2}^{1/2}\mathrm{d}\bar{\eta}, \end{aligned} \tag{27}$$

$$C_{33} = \frac{2m\pi\beta_y{}^2}{E'b}\int_0^{\bar{a}} F_{\mathrm{III}}(\bar{\xi})^2\bar{\xi}\mathrm{d}\bar{\xi}\int_{-1/2}^{1/2}\mathrm{d}\bar{\eta}, \tag{28}$$

$$C_{44} = \frac{2\pi}{E'b}\int_0^{\bar{a}}\left[m\phi_z{}^2F_{\mathrm{III}}(\bar{\xi})^2 + \phi_y{}^2F_{\mathrm{II}}(\bar{\xi})^2\right]\bar{\xi}\mathrm{d}\bar{\xi}\int_{-1/2}^{1/2}\mathrm{d}\bar{\eta}, \tag{29}$$

$$\begin{aligned} C_{55} &= \frac{288\pi}{E'b^3}\int_0^{\bar{a}} F_1(\bar{\xi})^2\bar{\xi}\mathrm{d}\bar{\xi}\int_{-1/2}^{1/2}\bar{\eta}^2\mathrm{d}\bar{\eta}, \\ C_{66} &= \frac{72\pi}{E'bh^2}\int_0^{\bar{a}} F_2(\bar{\xi})^2\bar{\xi}\mathrm{d}\bar{\xi}\int_{-1/2}^{1/2}\mathrm{d}\bar{\eta}, \end{aligned} \tag{30}$$

$$\begin{aligned} C_{15} &= \frac{24\pi}{E'b^2}\int_0^{\bar{a}} F_1(\bar{\xi})^2\bar{\xi}\mathrm{d}\bar{\xi}\int_{-1/2}^{1/2}\bar{\eta}\mathrm{d}\bar{\eta}, \\ C_{16} &= \frac{12\pi}{E'bh}\int_0^{\bar{a}} F_1(\bar{\xi})F_2(\bar{\xi})\bar{\xi}\mathrm{d}\bar{\xi}\int_{-1/2}^{1/2}\mathrm{d}\bar{\eta}, \end{aligned} \tag{31}$$

$$\begin{aligned} C_{24} &= \frac{2\pi\phi_y\beta_z}{E'b}\int_0^{\bar{a}} F_{\mathrm{II}}(\bar{\xi})^2\bar{\xi}\mathrm{d}\bar{\xi}\int_{-1/2}^{1/2}\mathrm{d}\bar{\eta}, \\ C_{34} &= \frac{2m\pi\phi_z\beta_y}{E'b}\int_0^{\bar{a}} F_{\mathrm{III}}(\bar{\xi})^2\bar{\xi}\mathrm{d}\bar{\xi}\int_{-1/2}^{1/2}\mathrm{d}\bar{\eta}, \end{aligned} \tag{32}$$

$$C_{56} = \frac{144\pi}{E'b^2h}\int_0^{\bar{a}} F_1(\bar{\xi})F_2(\bar{\xi})\bar{\xi}\mathrm{d}\bar{\xi}\int_{-1/2}^{1/2}\bar{\eta}\mathrm{d}\bar{\eta}, \tag{33}$$

where $\bar{a} = a/h$, $\bar{\eta} = \eta/b$. Substituting equations (22)–(25) into equations (27)–(33), the local flexibility coefficients can be evaluated by numerical integration method.

Then, the local additional flexibility matrix caused by the crack can be written as

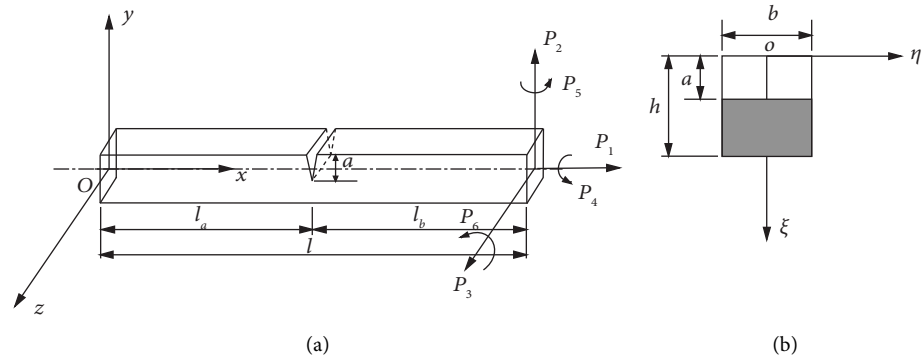

(a) (b)

FIGURE 2: The cracked structural member with rectangular cross section. (a) The cracked structural member, (b) local coordinate system of the cross section at the crack position.

$$\mathbf{C}_C = \begin{bmatrix} C_{11} & 0 & 0 & 0 & C_{15} & C_{16} \\ & C_{22} & 0 & C_{24} & 0 & 0 \\ & & C_{33} & C_{34} & 0 & 0 \\ & & & C_{44} & 0 & 0 \\ & \text{sym} & & & C_{55} & C_{56} \\ & & & & & C_{66} \end{bmatrix}. \tag{34}$$

Note that, different from the additional flexibility matrix in Reference [3] which omitted the coefficients C_{22}, C_{33}, C_{24}, and C_{34} considering the length of the member is very large compared to its transverse dimensions, here a complete additional flexibility matrix is derived.

Using the local additional flexibility matrix $\mathbf{C}_C$, the stiffness matrix of the elastic connection element for the crack can be evaluated as

$$\mathbf{S}_C = \mathbf{T}\mathbf{C}_C^{-1}\mathbf{T}^{\mathrm{T}}, \tag{35}$$

where

$$\mathbf{T} = \begin{bmatrix} -\mathbf{I} \\ \mathbf{I} \end{bmatrix}. \tag{36}$$

$\mathbf{I}$ is a 6×6 identity matrix.

2.3. Spectral Element Model of the Cracked Structural Member. Assembling the spatial beam elements and the elastic connection element as shown in Figure 1, the equation of motion of the four-node spectral element model for the cracked structural member can be obtained as

$$\mathbf{S}_M(s)\mathbf{u}_M(s) = \mathbf{F}_M(s). \tag{37}$$

Assuming the internal nodes m and n are not subjected to driving forces, equation (37) can be rewritten as the following block matrix form

$$\begin{bmatrix} \mathbf{S}_{M11} & \mathbf{S}_{M12} \\ \mathbf{S}_{M21} & \mathbf{S}_{M22} \end{bmatrix} \begin{Bmatrix} \mathbf{u}_{M1} \\ \mathbf{u}_{M2} \end{Bmatrix} = \begin{Bmatrix} \mathbf{F}_{M1} \\ \mathbf{0} \end{Bmatrix}, \tag{38}$$

where $\mathbf{u}_{M1}$ is composed of the displacement vectors of nodes i and j, $\mathbf{u}_{M2}$ is composed of the displacement vectors of nodes m and n, $\mathbf{S}_{M11}$, $\mathbf{S}_{M12}$, $\mathbf{S}_{M21}$, and $\mathbf{S}_{M22}$ are submatrices of the matrix $\mathbf{S}_M$.

Using the dynamic condensation method [42], a two-node condensed spectral element model can be obtained for the cracked structural member with the dynamic stiffness matrix

$$\mathbf{S}_M^* = \mathbf{S}_{M11} - \mathbf{S}_{M12}\mathbf{S}_{M22}^{-1}\mathbf{S}_{M21}. \tag{39}$$

2.4. Calculation of the Wave Response. For structure composed of multiple structural members, the spectral element equation of the structure can be obtained by assembling the spectral element matrix of each member obtained in equation (39)

$$\mathbf{S}(s)\mathbf{u}(s) = \mathbf{F}(s), \tag{40}$$

where $\mathbf{S}$ is the spectral element matrix of the whole structure, $\mathbf{u}$ and $\mathbf{F}$ are the nodal displacement vector and nodal load vector of the whole structure after Laplace transformation, respectively. Then, the boundary conditions of the structure can be implemented on equation (40) by the approaches as used in conventional FEM method [43].

For structural damage detection using the ultrasonic guided wave method, the sinusoidal wave signal tuned by Hanning window is usually selected as the narrow-band impulse excitation signal [44, 45] which can be expressed as

$$\begin{aligned} F(t) = F_0 &\left[\mathrm{He}(t-\tau) - \mathrm{He}\left(t - \tau - \frac{n}{f} \right) \right] \\ &\cdot \left[1 - \cos\left(\frac{2\pi f}{n} t \right) \right] \sin(2\pi f t), \end{aligned} \tag{41}$$

where $\mathrm{He}(t)$ is the step function, n is the number of peaks, f is the central frequency, and τ is the time constant for adjusting the position of the pulse signal.

The Laplace transformation of equation (41) can be obtained by using the mathematic software such as Maple, taking $n = 5$ as an example, its Laplace transformation is

$$\widehat{F}(s) = F_0\left[e^{(-s\tau-5s)/f} - e^{-s\tau}\right]\frac{A}{B}, \tag{42}$$

where

$$\begin{aligned} A = {} & \left[5\left(4\pi^2 f^2 + s^2\right)(8\cos(1.6\pi f\tau)\pi f + 5\sin(1.6\pi f\tau)s) - 2\left(64\pi^2 f^2 + 25s^2\right)\right. \\ & \cdot (2\cos(2\pi f\tau)\pi f + \sin(2\pi f\tau)s)] \cdot \left(144\pi^2 f^2 + 25s^2\right) \\ & + 5[12\cos(2.4\pi f\tau)\pi f + 5\sin(2.4\pi f\tau)s] \cdot \left(4\pi^2 f^2 + s^2\right)\left(64\pi^2 f^2 + 25s^2\right), \\ B = {} & 2\left(144\pi^2 f^2 + 25s^2\right)\left(4\pi^2 f^2 + s^2\right)\left(64\pi^2 f^2 + 25s^2\right). \end{aligned} \tag{43}$$

From equation (40), the wave response of the structure in Laplace domain can be evaluated. Then, the wave response in time domain can be obtained by using the inverse Laplace transformation. Taking the axial displacement u_j of node j as an example,

$$u_j(t) = \frac{1}{2\pi \mathrm{i}}\int_{\sigma-\mathrm{i}\infty}^{\sigma+\mathrm{i}\infty} \widehat{u}_j(s)e^{st}\mathrm{d}s, \tag{44}$$

where $\widehat{u}_j(s)$ is the axial displacement response of node j in Laplace domain.

Considering that $\widehat{u}_j(s)$ calculated by SEM is a group of discrete data, equation (44) can be carried out by the numerical inverse Laplace transformation (NILT) method. Specifically, the NILT algorithm proposed in [46] can be used.

3. Numerical Examples

Consider a steel structural member with rectangular cross section, the length of the member is $L = 0.4$ m, the width and height of its cross section are $b = h = 10$ mm. The elastic modulus, density and Poisson's ratio of the material are $E = 210$ GPa, $\rho = 7860$ kg/m^3, and $\nu = 0.3$, respectively. Assuming that the center of the crack is 0.2 m away from the left end of the structural member.

In this study, the parameters of the excitation signal in equation (41) are set as $F_0 = 1000$ N, $f_0 = 100$ kHz, $n = 5$ and $\tau = 0$. The time history and frequency spectrum of this excitation signal are shown in Figure 3.

In order to verify the calculation results of the presented spectral element model, the 3D finite element model of structural member was established by ANSYS software. The FEM model was meshed with Solid185 element. For accurately simulating the propagation of ultrasonic guided waves in the structure, the element size must be very small. In this example the element size in the axil direction of the member is taken as 0.4 mm, and the element size in the height and width directions of the cross section is taken as 1 mm. The FEM model of the structural member with crack depth $a = 0.5h = 5$ mm is shown in Figure 4, this model has 120912 nodes and 99800 elements. Considering the central frequency of the excitation signal and the computational cost, after a trial calculation with different time steps ($\Delta t = 1\times10^{-6}$ s, 1×10^{-7} s and 1×10^{-8} s), the time step used in the simulation of ANSYS model is selected as 1×10^{-7} s.

Firstly, the accuracy of the presented modeling method for uncracked structural member will be checked. Considering the member is clamped at the left end and free at the right end, the impulse excitation is applied as an area load on the right end face of the member along the axial direction, and the propagation of longitudinal wave in the member is investigated. Figure 5 shows the axial displacement response of the node at the center of the right end face of the member. As can be seen from Figure 5, for the propagation of longitudinal waves in the cantilevered uncracked structural member, the displacement response can be accurately obtained by using the SEM model based on the Love rod theory, while the result of the SEM model based on the elementary rod theory has an obvious error on the arriving time and wave form of the reflected waves.

To investigate the propagation of flexural wave in the uncracked member, the impulse excitation is applied as a line load on the edge of the right end face of the member along the vertical direction. Figure 6 shows the transverse displacement response of the node at the center of the right end cross section of the member. It can be seen that for the propagation of high-frequency flexural wave in the cantilevered uncracked structural member, the wave response can be accurately obtained by using the SEM model based on the modified Timoshenko beam theory (the adjustment coefficient η_1 in equation (9) is selected as 1.05 after a trial calculation), while the result of the SEM model based on the classical Timoshenko beam theory has an obvious error on the arriving time of the reflected wave.

Next, the accuracy of the presented modeling method for the cantilevered cracked member will be verified. The crack depth is assumed as $a = 0.5h$, and the impulse excitation is applied at the freed end along the axial direction. Figure 7 shows the axial and transverse displacements of the node at the center of the free end of the cracked member under the axial impulse excitation. It can be found that due to the stiffness coupling effect caused by the crack, the flexural wave is generated when the longitudinal wave reaches the crack, and the transverse displacement caused by the flexural wave has the same order of magnitude with the axial displacement caused by the longitudinal wave. Comparing the calculation results of the SEM model and the ANSYS FEM model, it can be found that the results of the presented SEM model considering the stiffness coupling effect caused by the crack are in good agreement with the results of FEM model,

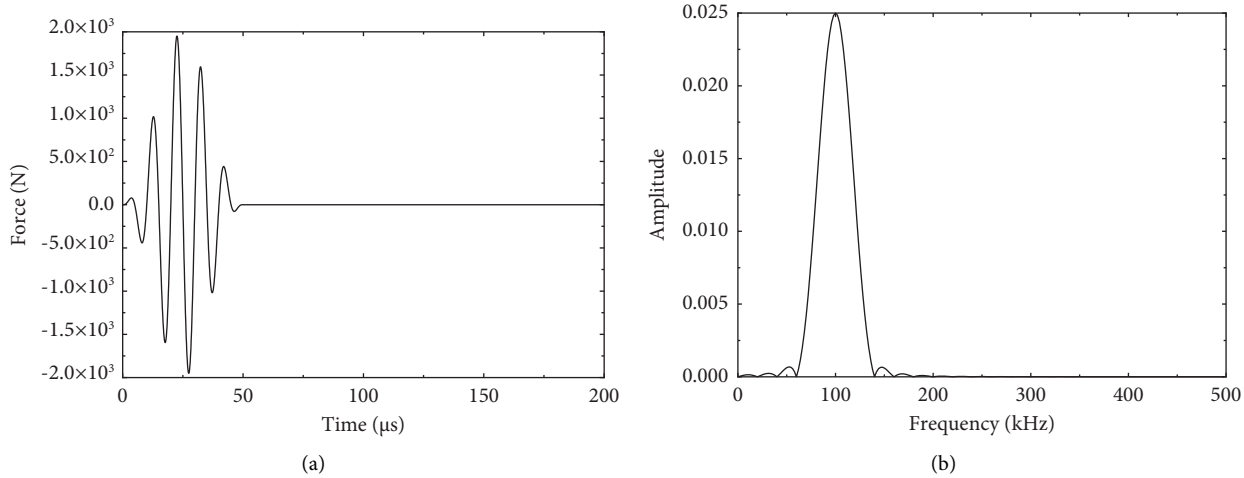

Figure 3: Narrow-band impulse excitation signal. (a) Time history, (b) frequency spectrum.

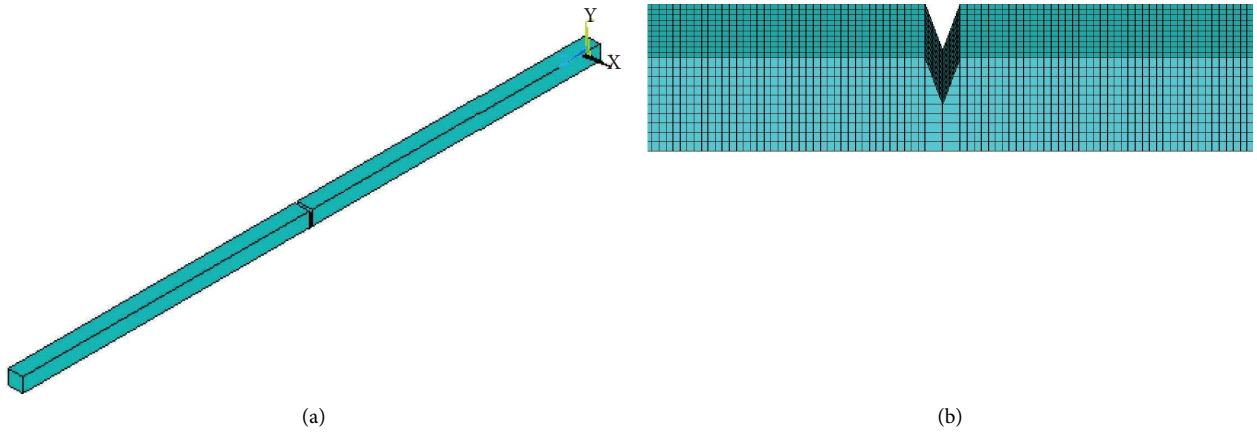

Figure 4: ANSYS model of the cracked member with crack depth $a = 0.5h$. (a) Geometrical model, (b) local part of the FEM model.

but if the stiffness coupling effect is neglected in the SEM model, the transverse displacement cannot be obtained from the SEM model, and the axial displacement obtained by the SEM model also has an obvious error. The above-given results indicate that the stiffness coupling effect caused by the crack should not be neglected in the wave propagation analysis of the cracked structures. Besides, the flexural wave response caused by the stiffness coupling is very useful in the crack identification [41].

In order to verify the accuracy of the presented modeling method for cracked member with various crack depth, another two crack depths are simulated, i.e., $a = 0.25h = 2.5$ mm (for a shallow crack) and $a = 0.75h = 7.5$ mm (for a deep crack). Figures 8 and 9 show the axial and transverse displacements of the node at the center of the free end of the cantilevered cracked member under the axial impulse excitation. It can be found that the presented method also gives accurate results for the structural member with both shallow and deep cracks.

The influence of crack width on the accuracy of the modeling method is investigated next. Four cases of crack widths are considered, i.e., 1 mm, 2 mm, 4 mm, and 8 mm, while the crack depth is $a = 0.5h = 5$ mm for all four cases. Since the flexibility coefficients of the crack evaluated by the strain energy release rate is independent of crack width, the wave responses evaluated by the presented SEM model for different crack width have no differences. In order to check the influence of crack width on the wave responses, the axial displacements at the free end of the cantilevered cracked member under the axial impulse excitation applied at its free end were evaluated by ANSYS model, which are shown in Figure 10. It can be found that the wave responses of these four cases have very slightly differences, which mean that the wave response is very insensitive to the crack width and the presented modeling method can be used for simulation of cracked structural member with different crack widths.

Furthermore, in order to check the applicability of the presented modeling method for cracked members with various boundary conditions, the cracked member with free-free boundary condition is considered here. The depth of the crack is assumed as $a = h/2$, and the impulse excitation is applied to one end face of the member along the axial direction. Figure 11 shows the axial and transverse displacement responses of the node at the center of the end face of

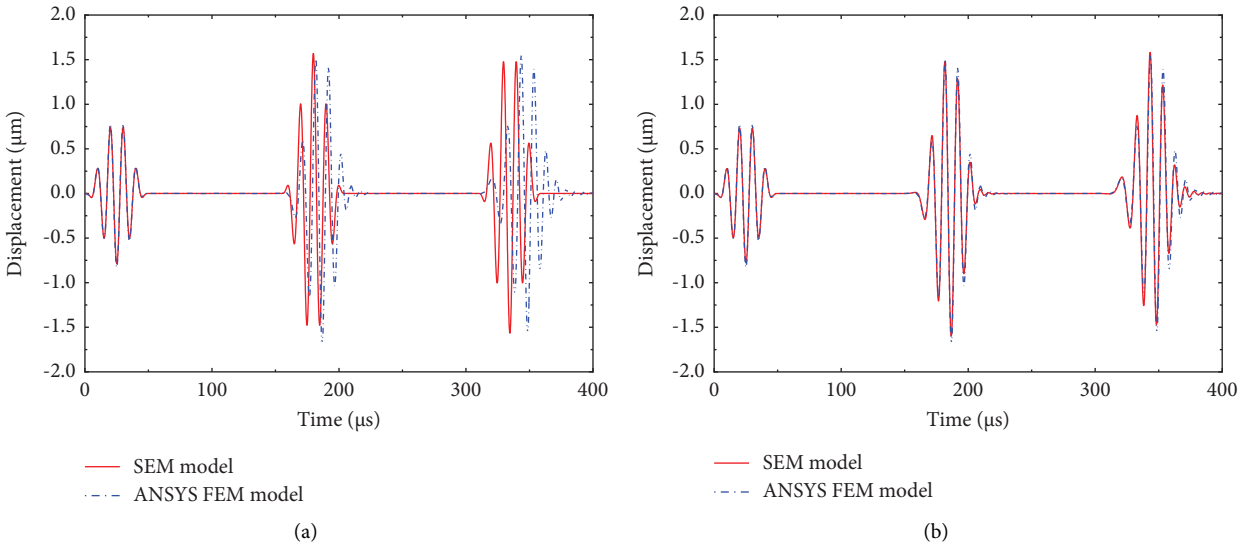

FIGURE 5: Calculation results of longitudinal wave propagation in the cantilevered uncracked member. (a) The result of elementary rod model, (b) the result of love rod model.

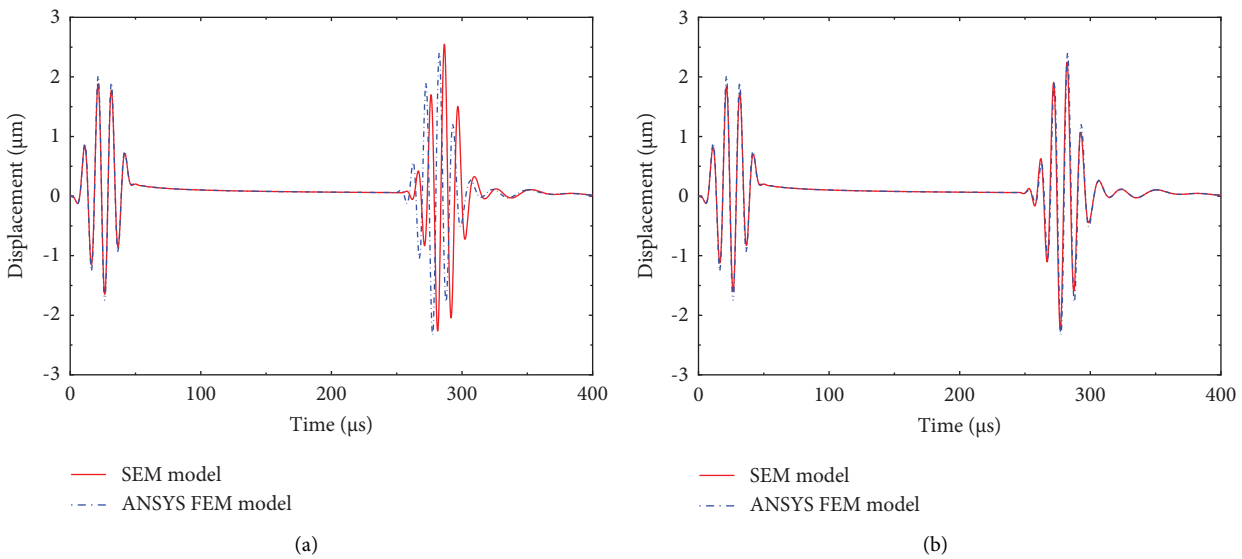

FIGURE 6: Calculation results of flexural wave propagation in the cantilevered uncracked member. (a) The result of classical Timoshenko beam model, (b) the result of modified Timoshenko beam model.

the cracked member under the impulse excitation. It can be seen that for the propagation analysis of ultrasonic guided waves in free-free cracked member, the calculation results of the presented SEM model are also in good agreement with the results of FEM model.

From the above-given comparisons between the presented SEM model and the 3D solid FEM model, it can be found that the presented SEM model can obtain accurate wave responses in simulation of cracked slender structures. The vast advantage of the SEM model is its extremely high computational efficiency. The SEM model in this example only uses one element, while the solid FEM model uses 99800 elements. The run of the MATLAB program of the SEM model and the analysis of the ANSYS solid FEM model was performed in a same computer (with AMD Ryzen 5 4600H processor, 16 GB RAM), the computational time of the SEM model is about 10 s, while the ANSYS solid FEM model needs about 10 hours.

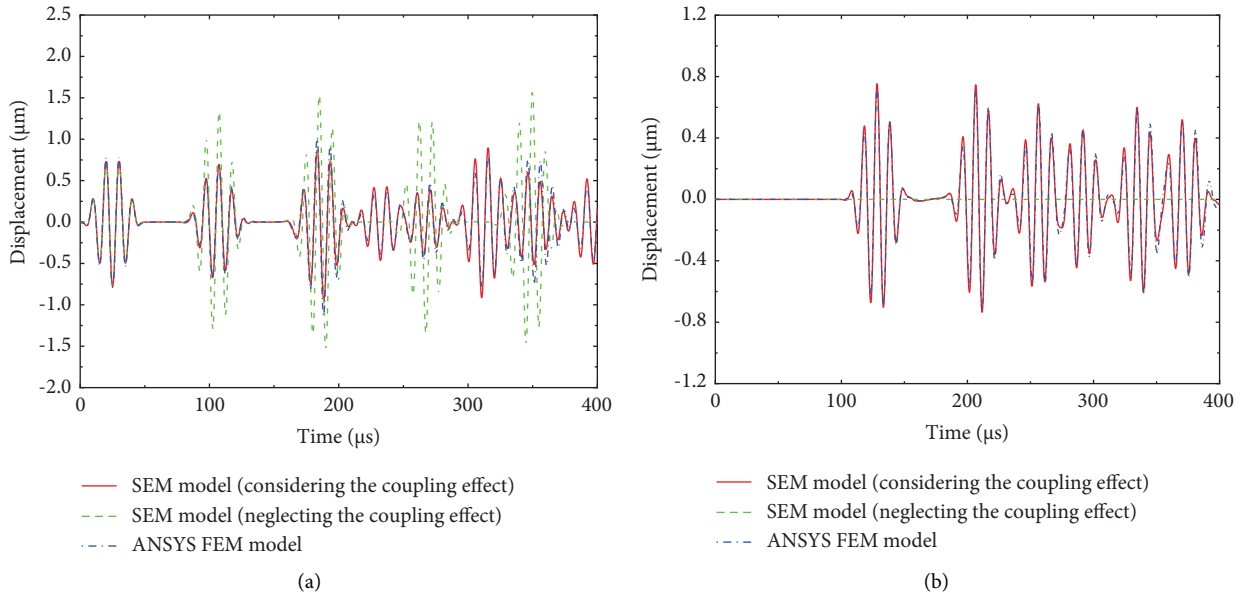

FIGURE 7: Calculation results of wave propagation in the cantilevered cracked structural member (the depth of the crack $a = 0.5h$). (a) Axial displacement, (b) transverse displacement.

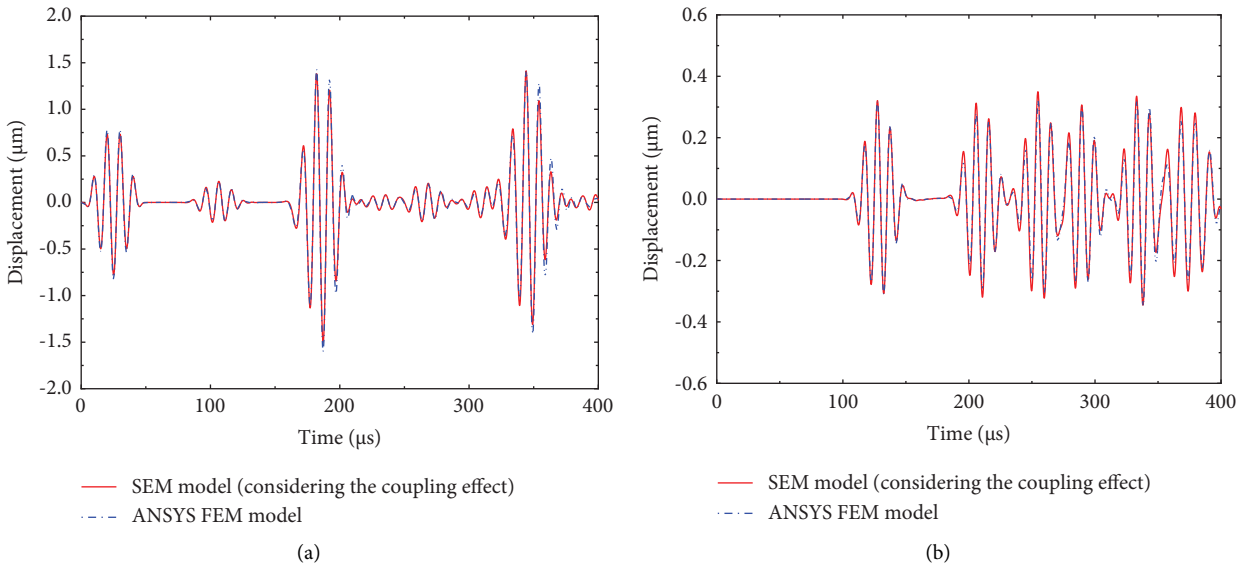

FIGURE 8: Calculation results of wave propagation in the cantilevered cracked structural member (the crack depth $a = 0.25h$). (a) Axial displacement, (b) transverse displacement.

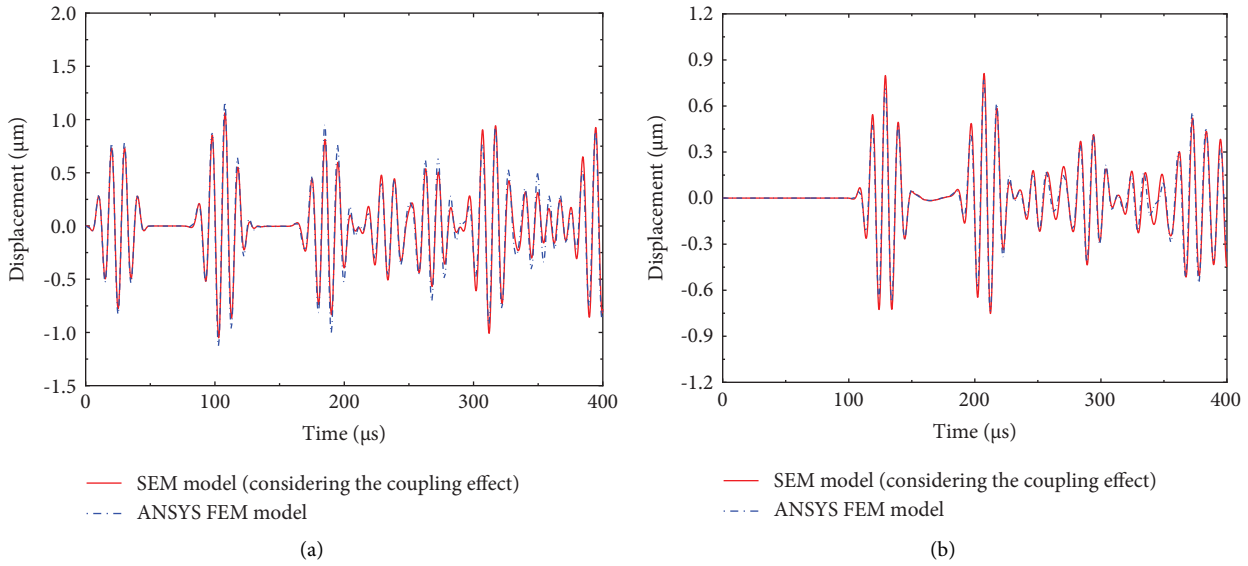

Figure 9: Calculation results of wave propagation in the cantilevered cracked structural member (the crack depth $a = 0.75h$). (a) Axial displacement, (b) transverse displacement.

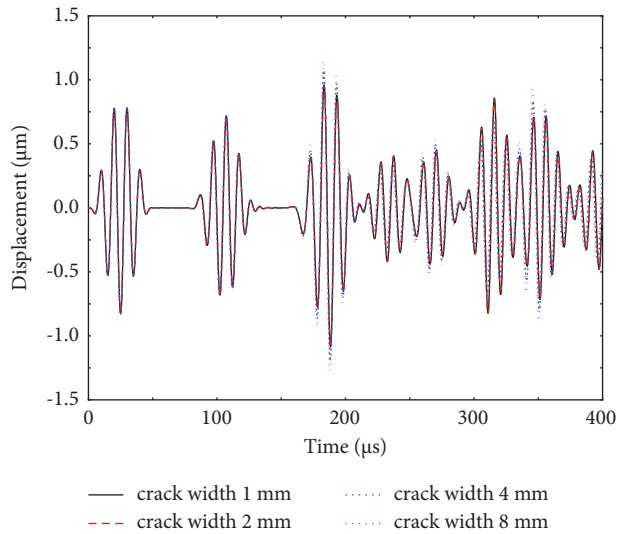

Figure 10: Influence of crack width on the wave response in the cantilevered cracked structural member (the crack depth $a = 0.5h$).

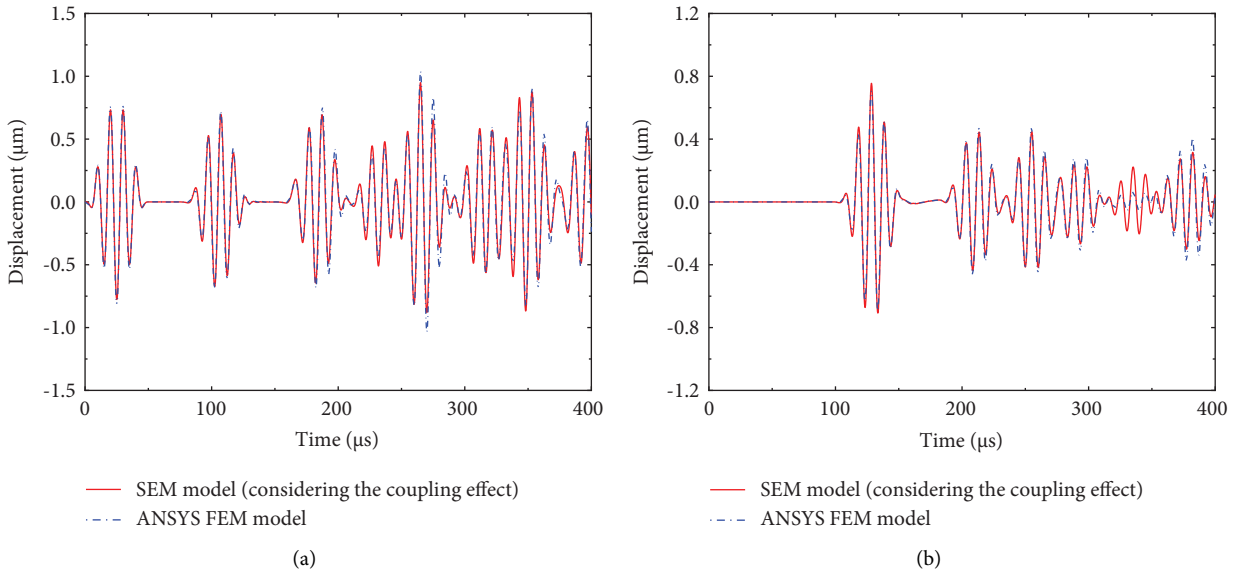

FIGURE 11: Calculation results of wave propagation in the free-free cracked structural member (the crack depth $a = 0.5h$). (a) Axial displacement, (b) transverse displacement.

4. Conclusions

An accurate modeling method for simulating wave propagation in cracked structural members was presented in this paper based on the spectral element method, and the propagation of ultrasonic guided wave in cracked structural member was analyzed by this model. By comparing the results of the spectral element model and the ANSYS 3D solid finite element model, it was found that the spectral element model based on the elementary rod theory and the classical Timoshenko beam theory has inevitable error in simulating the propagation of high-frequency elastic wave in structural member, while the spectral element model based on the Love rod theory and the modified Timoshenko beam theory can obtain more accurate results. The narrow-band impulse excitation applied in the axial direction of the structural member produces both of longitudinal wave and flexural wave in the structural member, and the transverse displacement caused by the flexural wave has the same order of magnitude with the axial displacement caused by the longitudinal wave. The crack depth has a significant effect on the wave response, while the crack width has negligible effect on the wave response. For simulating the propagation of ultrasonic guided wave in cracked structural members, the local stiffness coupling effect caused by cracks should be considered; otherwise, the calculation results will be inaccurate.

Data Availability

The data used to support the study are available from the corresponding author upon request.

Conflicts of Interest

The authors declare that they have no conflicts of interest.

Acknowledgments

This work was supported by the National Natural Science Foundation of China (Grant nos. 12172181 and 51778300), the Key Research and Development Project of Jiangsu Province (Grant no. BE2020703).

References

[1] S. H. Hsu, T. W. Chang, and C. M. Chang, "Impacts of label quality on performance of steel fatigue crack recognition using deep learning-based image," *Smart Structures and Systems*, vol. 29, no. 1, pp. 207–220, 2022.

[2] S. H. Hsu, H. T. Hung, and Y. Q. Lin, "Defect inspection of indoor components in buildings using deep learning object detection and augmented reality," *Earthquake Engineering and Engineering Vibration*, vol. 22, no. 1, pp. 41–54, 2021.

[3] P. N. Saavedra and L. A. Cuitino, "Crack detection and vibration behavior of cracked beams," *Computers & Structures*, vol. 79, no. 16, pp. 1451–1459, 2001.

[4] Q. Q. Wu, S. P. Guo, X. J. Li, and G. Gao, "Crack diagnosis method for a cantilevered beam structure based on modal parameters," *Measurement Science and Technology*, vol. 31, no. 3, Article ID 035001, 2020.

[5] J. Prawin, "Real-time reference-free breathing crack identification using ambient vibration data," *Structural Control and Health Monitoring*, vol. 29, no. 3, Article ID e2903, 2022.

[6] S. He and C.-T. Ng, "Guided wave-based identification of multiple cracks in beams using a Bayesian approach," *Mechanical Systems and Signal Processing*, vol. 84, pp. 324–345, 2017.

[7] X. Zhu and P. Rizzo, "Sensor array for the health monitoring of truss structures by means of guided ultrasonic waves," *Journal of Civil Structural Health Monitoring*, vol. 4, no. 3, pp. 221–234, 2014.

[8] R. Q. Guan, Y. Lu, K. Wang, and Z. Su, "Fatigue crack detection in pipes with multiple mode nonlinear guided waves," *Structural Health Monitoring*, vol. 18, no. 1, pp. 180–192, 2018.

[9] Y. P. Zhu, F. C. Li, and W. J. Bao, "Fatigue crack detection under the vibration condition based on ultrasonic guided waves," *Structural Health Monitoring*, vol. 20, no. 3, pp. 931–941, 2019.

[10] F. C. Li, H. G. Li, J. X. Qiu, and G. Meng, "Guided wave propagation in H-beam and probability-based damage localization," *Structural Control and Health Monitoring*, vol. 24, no. 5, Article ID e1916, 2017.

[11] M. Shamshirsaz, F. Bakhtiari-Nejad, M. Khelghatdoost, and S. Asadi, "Analytical and experimental analysis of Lamb wave generation in piezoelectrically driven Timoshenko beam," *Journal of Intelligent Material Systems and Structures*, vol. 26, no. 17, pp. 2314–2321, 2014.

[12] D. D. Chen, Z. H. Shen, R. L. Fu, B. Yuan, and L. Huo, "Coda wave interferometry-based very early stage bolt looseness monitoring using a single piezoceramic transducer," *Smart Materials and Structures*, vol. 31, no. 3, Article ID 035030, 2022.

[13] M. A. Majeed, M. Al-Ajmi, and A. Benjeddou, "Semi-analytical free-vibration analysis of piezoelectric adaptive beams using the distributed transfer function approach," *Structural Control and Health Monitoring*, vol. 18, no. 7, pp. 723–736, 2011.

[14] C. A. Papadopoulos and A. D. Dimarogonas, "Coupled longitudinal and bending vibrations of a rotating shaft with an open crack," *Journal of Sound and Vibration*, vol. 117, no. 1, pp. 81–93, 1987.

[15] D. Y. Zheng and N. J. Kessissoglou, "Free vibration analysis of a cracked beam by finite element method," *Journal of Sound and Vibration*, vol. 273, no. 3, pp. 457–475, 2004.

[16] G. Muscolino and R. Santoro, "Dynamics of multiple cracked prismatic beams with uncertain-but-bounded depths under deterministic and stochastic loads," *Journal of Sound and Vibration*, vol. 443, pp. 717–731, 2019.

[17] M. Mousavi, D. Holloway, J. C. Olivier, and A. H. Gandomi, "Quaternion analysis of beam multi-type vibration data for damage detection," *Structural Control and Health Monitoring*, vol. 29, no. 2, Article ID e2867, 2022.

[18] Y. Chai, W. Li, and Z. Liu, "Analysis of transient wave propagation dynamics using the enriched finite element method with interpolation cover functions," *Applied Mathematics and Computation*, vol. 412, Article ID 126564, 2022.

[19] J. F. Doyle, *Wave Propagation in Structures*, Springer Nature Switzerland AG, Basel, Switzerland, 3rd edition, 2021.

[20] U. Lee, *Spectral Element Method in Structural Dynamics*, John Wiley & Sons (Asia), Hoboken, NJ, USA, 2009.

[21] H. Igawa, K. Komatsu, I. Yamaguchi, and T. Kasai, "Wave propagation analysis of frame structures using the spectral element method," *Journal of Sound and Vibration*, vol. 277, no. 4-5, pp. 1071–1081, 2004.

[22] M. Mitra and S. Gopalakrishnan, "Wavelet based spectral finite element for analysis of coupled wave propagation in higher order composite beams," *Composite Structures*, vol. 73, no. 3, pp. 263–277, 2006.

[23] Y. Wang, H. Hao, X. Q. Zhu, and J. Ou, "Spectral element modelling of wave propagation with boundary and structural discontinuity reflections," *Advances in Structural Engineering*, vol. 15, no. 5, pp. 855–870, 2012.

[24] M. Palacz and M. Krawczuk, "Analysis of longitudinal wave propagation in a cracked rod by the spectral element method," *Computers & Structures*, vol. 80, no. 24, pp. 1809–1816, 2002.

[25] R. L. Lucena and J. M. C. Dos Santos, "Structural health monitoring using time reversal and cracked rod spectral element," *Mechanical Systems and Signal Processing*, vol. 79, pp. 86–98, 2016.

[26] M. Krawczuk, M. Palacz, and W. Ostachowicz, "The dynamic analysis of a cracked Timoshenko beam by the spectral element method," *Journal of Sound and Vibration*, vol. 264, no. 5, pp. 1139–1153, 2003.

[27] Z. M. Xu, M. S. Cao, R. B. Bai, H. Xu, and W. Xu, "Evaluation of high-order modes and damage effects of multi-crack beams using enhanced spectral element method," *Journal of Vibration and Control*, vol. 24, no. 21, pp. 107754631774750–107754631775200, 2018.

[28] R. A. Izadifard, R. K. Ranjbar, and B. Mohebi, "Wave propagation in cracked frame structures by the spectral element method," *International Journal of Advanced Structural Engineering*, vol. 6, p. 59, 2014.

[29] S. Ritdumrongkul and Y. Fujino, "Identification of the location and size of cracks in beams by a piezoceramic actuator–sensor," *Structural Control and Health Monitoring*, vol. 14, no. 6, pp. 931–943, 2007.

[30] F. S. Liu, D. P. Jin, and H. Wen, "Optimal vibration control of curved beams using distributed parameter models," *Journal of Sound and Vibration*, vol. 384, pp. 15–27, 2016.

[31] B. Akgöz and Ö. Civalek, "Buckling analysis of functionally graded tapered microbeams via Rayleigh–Ritz method," *Mathematics*, vol. 10, no. 23, p. 4429, 2022.

[32] M. H. Jalaei, H. T. Thai, and Ö. Civalek, "On viscoelastic transient response of magnetically imperfect functionally graded nanobeams," *International Journal of Engineering Science*, vol. 172, Article ID 103629, 2022.

[33] F. S. Liu, L. B. Wang, D. P. Jin, X. Liu, and P. Lu, "Equivalent micropolar beam model for spatial vibration analysis of planar repetitive truss structure with flexible joints," *International Journal of Mechanical Sciences*, vol. 165, Article ID 105202, 2020.

[34] H. S. Yang, Y. L. Li, and F. H. Zhou, "Propagation of stress pulses in a Rayleigh-Love elastic rod," *International Journal of Impact Engineering*, vol. 153, Article ID 103854, 2021.

[35] S. S. Rao, *Vibration of Continuous Systems*, John Wiley & Sons, Hoboken, NJ, USA, 2007.

[36] M. Krawczuk, A. Zak, W. Ostachowicz, and M. P. Cartmell, "Propagation of elastic waves in beams - including damping effects," *Materials Science Forum*, vol. 441, pp. 179–186, 2003.

[37] M. R. Machado, S. Adhikari, and J. M. C. Dos Santos, "Spectral element-based method for a one-dimensional damaged structure with distributed random properties," *Journal of the Brazilian Society of Mechanical Sciences and Engineering*, vol. 40, no. 9, p. 415, 2018.

[38] I. Jang, I. Park, and U. Lee, "Spectral element modeling and analysis of the dynamics and guided waves in a smart beam with a surface-bonded PZT layer," *Journal of Mechanical Science and Technology*, vol. 28, no. 4, pp. 1229–1239, 2014.

[39] A. D. Nashif, D. I. G. Johnes, and J. P. Henderson, *Vibration Damping*, John Wiley & Sons Inc, Hoboken, NJ, USA, 1985.

[40] L. Cremer and B. A. T. Petersson, *Structure-Borne Sound: Structural Vibrations and Sound Radiation at Audio Frequencies*, Springer-Verlag Berlin Heidelberg, Heidelberg, Germany, 3rd edition, 2005.

[41] C. A. Papadopoulos, "The strain energy release approach for modeling cracks in rotors: a state of the art review," *Mechanical Systems and Signal Processing*, vol. 22, no. 4, pp. 763–789, 2008.

[42] A. Y. T. Leung, "An accurate method of dynamic condensation in structural analysis," *International Journal for*

Numerical Methods in Engineering, vol. 12, no. 11, pp. 1705–1715, 1978.

[43] S. S. Rao, *The Finite Element Method in Engineering*, Elsevier Science & Technology Books, Amsterdam, Netherlands, 6th edition, 2018.

[44] Z. B. Yang, X. F. Chen, X. Li, Y. Jiang, H. Miao, and Z. He, "Wave motion analysis in arch structures via wavelet finite element method," *Journal of Sound and Vibration*, vol. 333, no. 2, pp. 446–469, 2014.

[45] W. W. Zhang, H. Hao, J. Wu, J. Li, H. Ma, and C. Li, "Detection of minor damage in structures with guided wave signals and nonlinear oscillator," *Measurement*, vol. 122, pp. 532–544, 2018.

[46] L. Brancik, "Programs for fast numerical inversion of Laplace transforms in MATLAB language environment," in *Proceedings of the 7th Conference MATLAB'99*, pp. 27–39, Czech Republic, Prague, Europe, July 1999.